AIAA Aviation
22-26 June 2015, Dallas, TX
22nd AIAA Computational Fluid Dynamics Conference

Assessment of Hybrid RANS/LES Methods For Gas-Turbine Combustor-Relevant Turbulent Flows

Jonathan P. West * and Clinton P. T. Groth †
University of Toronto Institute for Aerospace Studies,
4925 Dufferin St., Toronto, Ontario, M3H 5T6, Canada

John T. C. Hu ‡
Pratt & Whitney Canada
1801 Courtneypark Dr., Mississauga, Ontario, L5T 1J3, Canada

In order to investigate the use of hybrid turbulence models utilizing both Reynolds-averaged Navier-Stokes (RANS) and large eddy simulation (LES) strategies, also known as hybrid RANS/LES, for turbulent gas-turbine combustor-relevant flows, numerical simulations for several representative/benchmark cold-flow cases were performed using a standalone RANS model, a detached eddy simulation (DES) model, a standalone LES model, and a so-called dynamic LES (DLES) model. Predictions of each model were compared to available experimental data. Through this process, the predictive performance of DES, a common hybrid RANS/LES method, was shown to be subject to several established deficiencies, such as modelled stress depletion (MSD) for some of the benchmark cases studied. These issues proved to be a disadvantage when compared to the other modelling strategies for cases with simple geometry and flow structures. However, it was shown that a fine pre-LES zone mesh could be used to manipulate MSD regions and improve DES performance. Additionally, the predictive performance of DES was significantly improved in comparison to the other treatment techniques for turbulence for cases with greater complexity in flow geometry and features, such as swirl. The latter are more representative of the turbulent flows of interest here.

I. Introduction and Motivation

As discussed by Wilcox[1], turbulence is a continuum phenomenon, the physics of which is captured by the Navier-Stokes equations without modelling. Simulating turbulent flows with the Navier-Stokes equations only would be ideal, practically however, it is to expensive computationally to resolve the Navier-Stokes equations over the whole range of turbulent scales for engineering problems. As a consequence, simulations of practical engineering problems require that turbulence must be modelled to some degree. Reynolds-averaged Navier-Stokes (RANS) methods provide a low computational cost and good near wall modelling but must model the full range of turbulent scales without resolving even large scale turbulent features. As a result, they often fail to properly capture information about unsteady flow features and turbulent mixing. Large eddy simulation (LES) methods only model turbulent structures on the smallest scales and resolve the remaining scales without modelling. However, LES methods can in many instances be computationally too expensive near walls for practical three-dimensional geometries unless paired with an empirical wall model, which is generally considered less sophisticated than a RANS model near walls as discussed by Fröhlich *et al.*[2]

Hybrid RANS/LES methods can potentially circumvent the weaknesses of standalone RANS and LES models by using LES outside of boundary layers and reserving RANS only for near wall and/or under resolved

*Ph.D. Candidate, Email: j.west@mail.utoronto.ca, and AIAA Student Member.
†Professor, Email: groth@utias.utoronto.ca , and AIAA Senior Member.
‡Manager, Hot Section Technology, Email: john.hu@pwc.ca.

Table 1. Validation cases considered in study.

Case	Mean Flow Dimensions	Flow Features				
		Re-circulation	Mixing	Swirl	Periodic Features	Complex Geometry
Backward facing step of Driver *et al.*[7]	2	yes				
Bluff body burner in co-flow of Dally *et al.*[8]	Axisymetric	yes				
Propane-jet in co-flow of Schefer[9]	Axisymetric		yes			
Hydrogen-jet in cross-flow of Steinberg *et al.*[10]	3		yes			
Bluff body flame stabilizer in duct of Sjunnesson *et al.*[11]	2			yes	yes	
Swirl stabilized combustor of Steinberg *et al.*[12]	3	yes		yes	yes	yes

regions. Hybrid RANS/LES modelling strategies has been widely applied for non-reacting flows, as discussed in a review by Fröhlich *et al.*[2] and for detached eddy simulation (DES) specifically as discussed in a review by Spalart[3]. These methods have also been applied to reacting flows in previous studies by Choi *et al.*[4] and Sainte-Rose *et al.*[5,6] and may have significant potential for predicting turbulent reactive flows in practical gas-turbine combustors. Nevertheless, their application to reactive flow simulation requires further study.

II. Scope of Present Study

In order to investigate the use of hybrid RANS/LES methods for turbulent combustor-relevant flows, several cold (non-reacting) flow configurations were selected as being representative of the flow types often encountered in practical gas-turbine combustion devices. Additionally, the cases were intended to represent a progressive increase in the complexity of the flow, from relatively simple turbulent flows to complex turbulent flows exhibiting a high degree of three-dimensionality, unsteadiness, and/or swirl. It was anticipated that this would demonstrate in an incremental fashion the advantages of the hybrid RANS/LES strategy over RANS as the complexity of the problem increased. The specific cases considered are summarized in Table 1 along with the relative complexity of the flow features. The selected cases are as follows:

- Backward facing step case of Driver *et al.*[7];
  - Classical boundary-layer separation caused by a vertical step followed be re-attachment downstream, generating a re-circulation zone.
- Bluff body burner in co-flow case of Dally *et al.*[8].
  - A pipe with a large outer diameter and small inner diameter injects a higher velocity air-jet into slower co-flowing air. The large outer diameter generates a re-circulation region between the co-flowing air and the central jet.
- Propane-jet in co-flow case of Schefer[9];
  - A propane jet is exhausted from a relatively skinny pipe into slower co-flowing air with no swirl.
- Hydrogen-jet in cross-flow case of Steinberg *et al.*[10];
  - A small diameter high velocity hydrogen-jet is injected into a rectangular air duct at an angle perpendicular to the slower flowing air.

- Bluff body flame stabilizer in duct flow case of Sjunnesson *et al.*[11]; and
  - A triangular obstruction in a rectangular duct with flowing air that generates vortices which shed periodically from the downstream corners of the obstruction.
- Swirl stabilized combustor case of Steinberg *et al.*[12];
  - A industry inspired plenum and swirler assembly generates a complex swirling non-reacting flow which enters a test section resembling a rectangular prism.

For comparative purposes, the selected cases were simulated not only with a hybrid RANS/LES method but, using the same mesh, with a RANS method, an LES method, and a so-called dynamic LES (DLES) method. The commercial code Ansys FLUENT was used as it includes implementations of all these approaches allowing for comparison with minimal change in the underlying numerical method. The specific turbulence models considered were as follows:

- RANS Model: Shear Stress Transport (SST) k-ω model of Menter *et al.*[13];
- DES Model: DES model derived from the SST k-ω RANS model of Menter *et al.*[13];
- LES Model: Smagorinsky-Lilly model as described in Piomelli *et al.*[14] with wall modelling; and
- DLES Model: DLES variant of the Smagorinsky-Lilly model as described in Germano *et al.*[15] with wall modelling.

Within the Ansys FLUENT solver, the SIMPLE algorithm of Patankar *et al.* [16] was utilized for pressure-velocity coupling and the second-order up-wind scheme of Barth *et al.* [17] for pressure interpolation. Time advancement was accomplished with second-order dual time stepping in which sub-iterations at each time step were used to converge temporally discretized equations.

III. DES Mesh Design and Analysis

Through a trial and error process, as well as based on some of the ideas described in previous work by Spalart[18], a procedure has been developed for arriving at appropriate computational meshes for conducting DES simulations. In what follows, the proposed meshing procedure is illustrated for the case of flow past the backward facing step of Driver *et al.*[7] In this case, a flow boundary layer detaches due to a vertical step and re-attaches downstream generating a stationary re-circulation zone. The size of this re-circulation zone can be characterized by the length required for the detached boundary layer to re-attach, known as the re-attachment length.

III.A. Initial Simulation

An initial RANS simulation should be conducted using a RANS designed mesh. A 2D simulation for cases with a statistically steady 2D or axisymmetric flow is sufficient. Using this simulation data, turbulent scale information can be estimated from the flow. In particular, the Taylor microscale and integral length scale profiles of the flow are useful in the mesh design process.

III.B. Preliminary Mesh Design

As recommended by Spalart[18], the flow domain and mesh style was divided into several regions based on the turbulence model intended to function in each region. These flow regions are described as follows:

- Euler regions: Non-turbulent, large cell sizes permissible;
- RANS regions: RANS meshing (high aspect ratio cells near walls);
- LES focus region: Isotropic mesh cells, LES mesh requirements; and
- LES departure region: Transition from focus region mesh to coarser mesh.

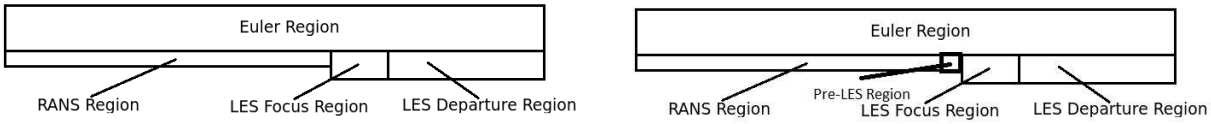

(a) Preliminary Mesh Plan (b) Pre-LES Zone Mesh Plan

Figure 1. Backward Facing Step DES Mesh Plans

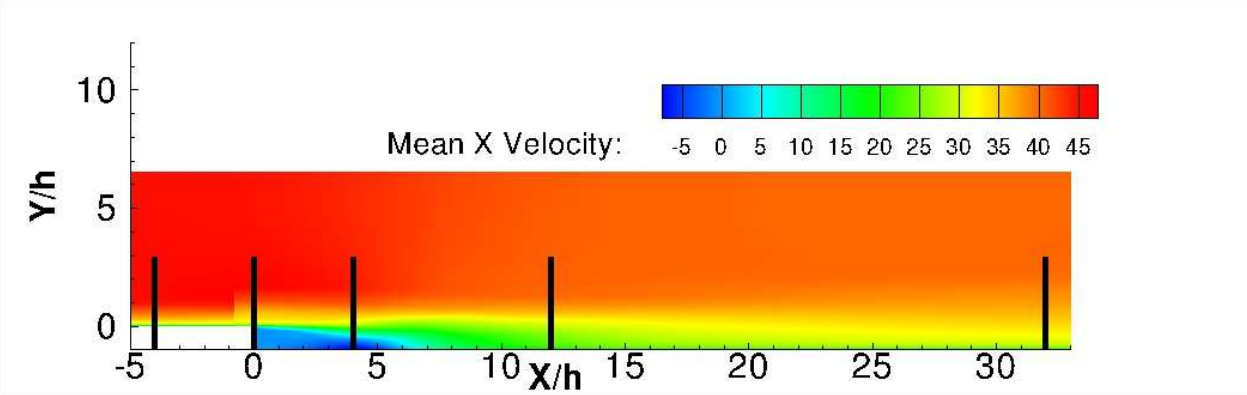

Figure 2. Results comparison stations (black) within the mean flow of the backward facing step case.

For the case of flow past a backward facing step, these regions of the DES computational domain are shown in Figure 1(a).

As can be seen in Figure 1(a), the LES focus region encompasses the recirculation zone and the detached boundary layer after the step. In the LES focus region isotropic mesh cells were used, these cells were an order of magnitude larger than the Taylor microscale in that region. Although the mesh cell size would ideally be of the same order of magnitude as the Taylor microscale, this was not possible due to computational constraints. Additionally, the 3D simulation width was chosen to be of the same order of magnitude as the integral length scale. The resulting structured mesh consisted of ∼800 000 cells. The time step was chosen to satisfy a CFL condition of unity given U_∞ and the cell size in the LES focus region. Transient simulations were conducted starting from a base RANS flow profile and time marched $T = 0.1695s \sim 5\,(L/U_\infty)$, where L is the simulation domain length in the streamwise direction, once to reach a fully developed flow state and once again to collect steady flow statistics.

III.B.1. Modelled Stress Depletion with Preliminary Mesh

All results for the backward facing step case presented in this study are scaled using the step height (h), which is 0.0127 m, for spacial dimensions. Velocity values are scaled using the inlet velocity, which is 44.2 m/s. Results were primarily compared in profile stations located within the flow as shown in Figure 2.

Using the preliminary mesh, a DES simulation predicted the re-attachment point as 10.13 h which is significantly larger than the experimental value of 6.26 ± 0.1 h[7]. This is likely because the transition from RANS to LES mode works by increasing the destruction of modelled turbulent kinetic energy (TKE) from a RANS region, until it more approximates a sub-grid scale model, without directly transferring that energy into the resolved scales of the LES region. The DES method relies on the resolved scale turbulence to develop naturally from the numerical variations in the solver in the absence of the RANS TKE. This results in a small region between RANS and LES modes where there is not enough modelled or resolved TKE. This phenomenon is well known in the literature as Modelled Stress Depletion (MSD)[3]. Although MSD is a problem in many DES simulations, it is clear from the X/h=4 station of Figure 3, which is within the re-circulation zone of the backward facing step, that the DES simulation on the preliminary mesh has neither sufficient resolved or modelled TKE.

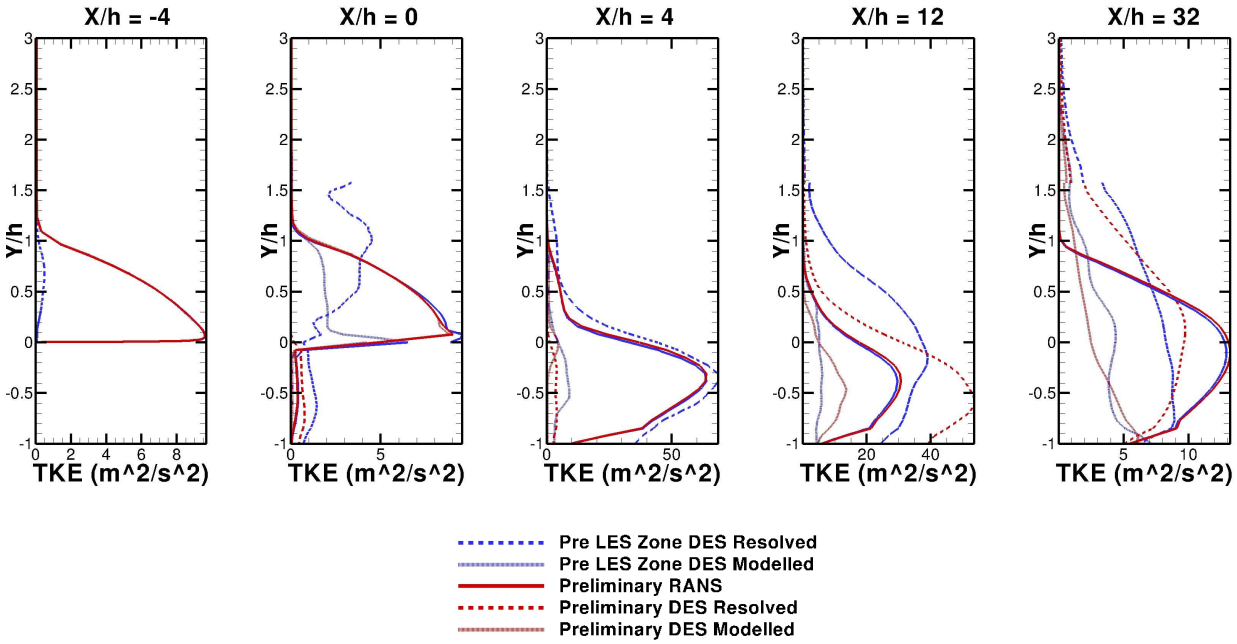

Figure 3. Backward Facing Step TKE Comparisons Between Solutions on Preliminary Mesh and Mesh with Pre-LES Zone

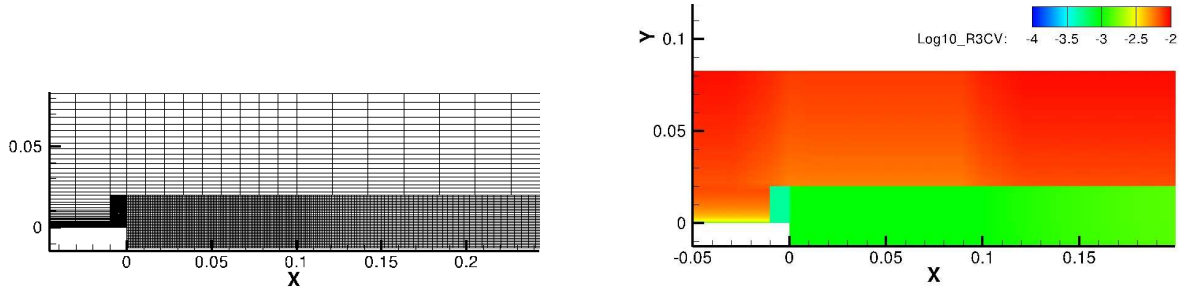

(a) Mesh

(b) Log10 of cubic root of cell volume contours.

Figure 4. Section of Backward Facing Step Mesh With Pre-LES Zone

III.C. Mesh with Pre-LES Zone

Various strategies were attempted to improve the performance of the DES method by altering the mesh. These strategies included extending the LES region farther upstream. The most effective strategy, however, was to create a small upstream region prior to the LES region of even finer mesh density located as shown in Figure 1(b). The pre-LES zone of this mesh can also be seen in Figure 4, which depicts the resulting structured computational mesh. This reduced mesh density facilitated the destruction of modelled TKE faster and in a different location. This changed the location of the MSD zone and reduced its size. As can be seen in Figure 3, the pre-LES mesh allowed the modelled DES TKE to be substantially dissipated by the beginning of the step (X/h=0) which allowed the resolved TKE to be fully developed within the re-circulation zone (X/h=4). In can also be seen that within the re-circulation zone and downstream of the re-circulation zone (X/h=4 and X/h=12) the DES resolved TKE, once developed, is significantly greater than the DES modelled TKE indicating that the LES region mesh is sufficiently fine. The resulting re-attachment length prediction was 5.91 h, which is within ∼0.5 h of the experimental result[7].

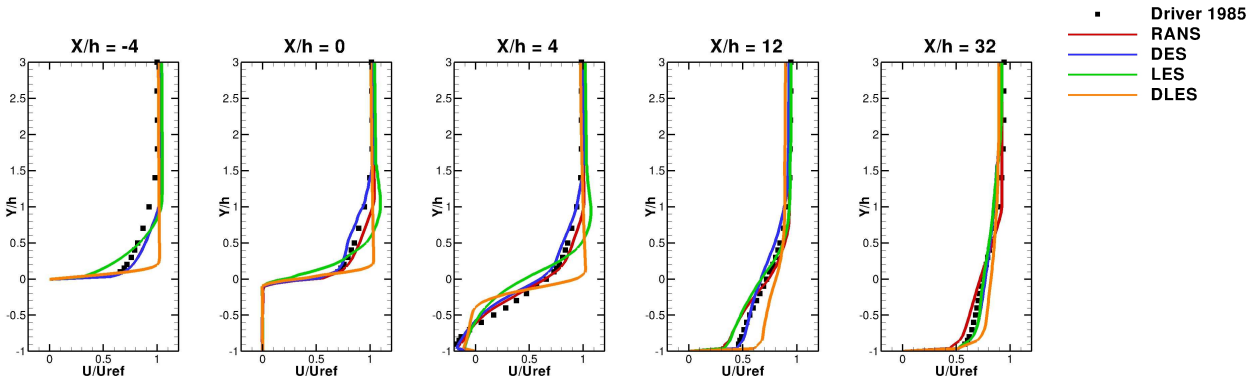

Figure 5. Backward facing step streamwise mean velocity comparisons.

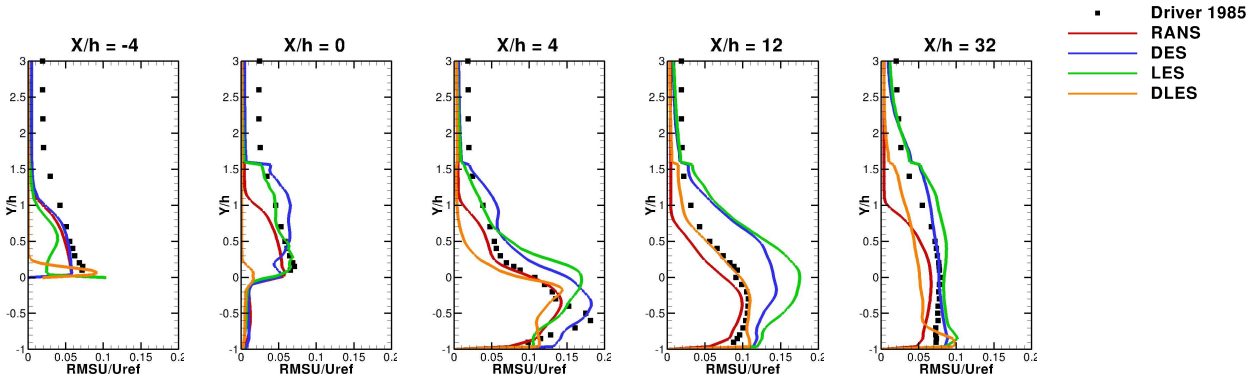

Figure 6. Backward facing step streamwise RMS velocity comparisons ($\tau_{ii}^{Modelled}$ included).

IV. Comparison of Numerical Results and Analyses

Utilizing the mesh design lessons discussed in Section III, a cost/benefit analysis of the DES method in comparison the other available stand-alone methods including RANS, LES, and DLES was conducted for the six selected validation cases.

IV.A. Backward Facing Step

The mesh for the backward facing step case that is described in Section III.C was also simulated using RANS, LES, and DLES. The time step used was chosen to satisfy a CFL condition of unity given U_∞ and the cell size in the LES focus region. Transient simulations were conducted starting from a base RANS flow profile and time marched $T = 0.1695s \sim 5\,(L/U_\infty)$, where L is the simulation domain length in the streamwise direction, once to reach a fully developed flow state and once again to collect steady flow statistics. These simulations were compared with experimental results from Driver *et al.*[7] along multiple stations in terms of streamwise velocity and streamwise root mean square (RMS) velocity as shown in Figures 5 and 6 respectively. The re-attachment lengths predicted by the different turbulence models are also presented in Table 2.

In terms of the streamwise velocity, as shown in Figure 5, DES works as intended by matching RANS results exactly prior to the step and matching experimental results well past the step. In terms of the streamwise RMS velocity, as shown in Figure 6, all methods considered were comparable, however, DLES matched experimental results best just past the step while DES matched experimental results best farther downstream. As can be seen in Table 2, all methods predicted the re-attachment point within ~0.5 h of the experimental results. Note that this flow case has a separation point prescribed by the geometry, and while involving separation, is a case a well-tuned RANS model can be expected to perform well. As illustrated by

Table 2. Backward facing step re-attachment lengths predicted by turbulence models.

Simulation	Re-Attachment Length (h)
RANS	6.30
DES	5.91
LES	6.38
DLES	6.54
Experiment	6.26 ± 0.1[7]

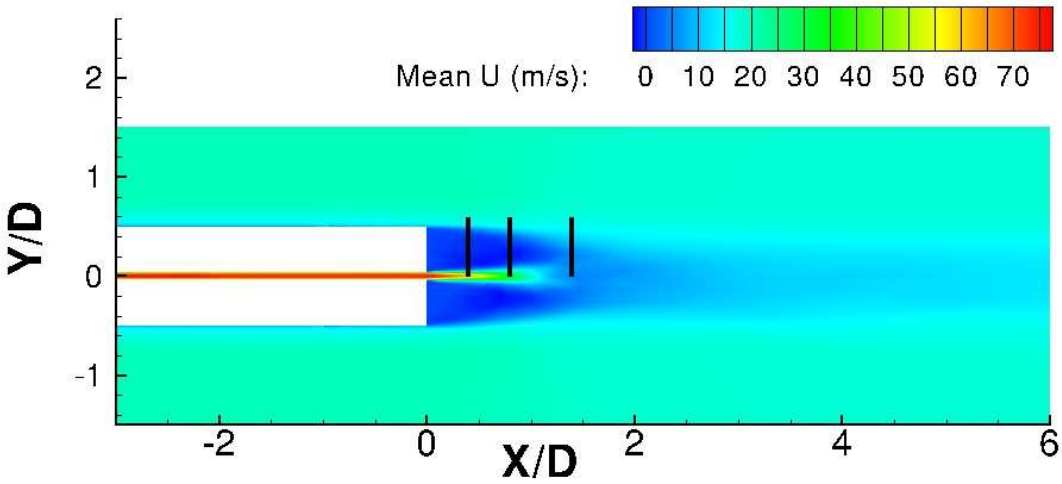

Figure 7. Results comparison stations (black) within the mean flow of the bluff body burner in cold-flow case.

the results, the RANS predictions are equal if not superior to its fully-unsteady counterparts for this case.

IV.B. Bluff Body Burner Cold-Flow

Several non-reacting air-jet data sets are available from experimentation with the bluff body burner apparatus of Dally *et al.*[8] In this flow case a pipe with a large outer diameter and small inner diameter injects a higher velocity air-jet into slower co-flowing air. The large outer diameter generates a re-circulation region between the co-flowing air and the central jet. This re-circulation influences the dispersion of the central jet. RANS, DES, LES, and DLES simulations were conducted for comparison on a structured mesh of 2 030 710 cells as shown in Figure 8. Transient simulations were conducted starting from a base steady RANS flow profile and time marched $T = 0.1s \sim 5\,(L/U_{co-flow})$, where L is the simulation domain length in the streamwise direction and $U_{co-flow}$ is the co-flow air velocity, once to reach a fully developed flow state and once again to collect steady flow statistics. The time step was chosen to satisfy a CFL condition of unity given U_{max} and the target cell size in the pre-LES region, where U_{max} is the highest velocity magnitude identified in the domain. This value was determined utilizing preliminary steady RANS simulations. A longer section of up-stream domain consistent with the experimental apparatus was simulated using steady RANS, velocity and turbulence property profiles from this steady simulation where used as inlet conditions for the transient simulations. Mean and RMS streamwise velocity profiles for the simulations are shown in Figures 9 and 10 respectively. Spatial dimensions were scaled using the bluff body diameter (D), which is 0.05 m or the bluff body radius (R), which is 0.025 m. Velocity and RMS velocity values were normalized by U_{jet}, which is 61 m/s. Results for this case were primarily compared in profile stations located within the flow as shown in Figure 7.

As can be seen in Figures 9 and 10, although DES performs very well compared to RANS and appears to have an advantage over LES and DLES, there does not appear to be any advantage offered by the hybrid treatment over conventional RANS.

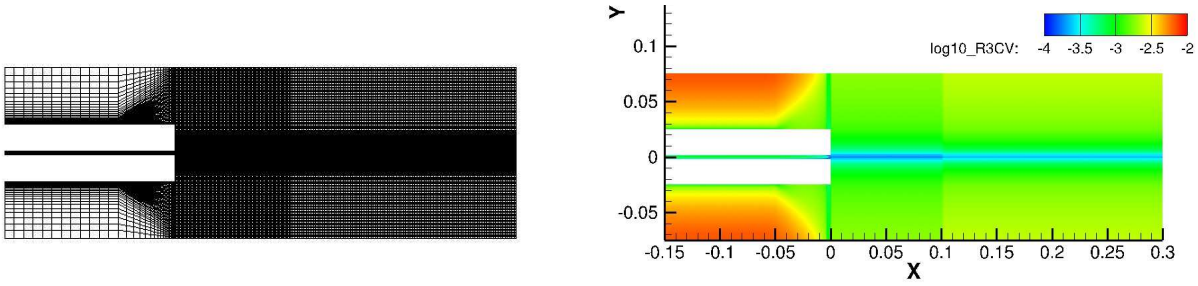

(a) Mesh.

(b) Log10 of cubic root of cell volume contours.

Figure 8. Bluff body burner cold-flow case mesh layout.

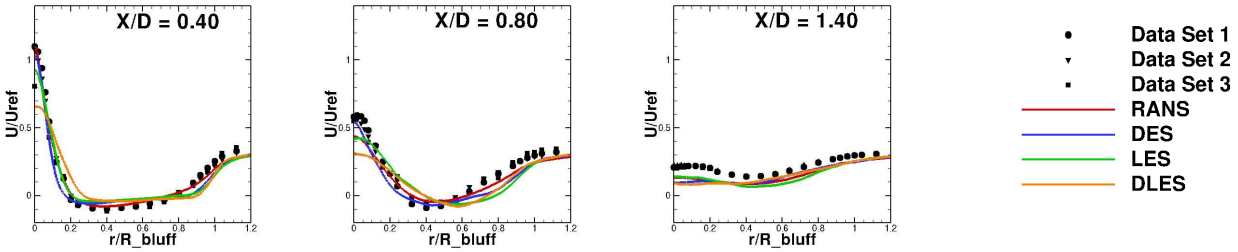

Figure 9. Bluff body burner cold-flow case streamwise velocity comparisons.

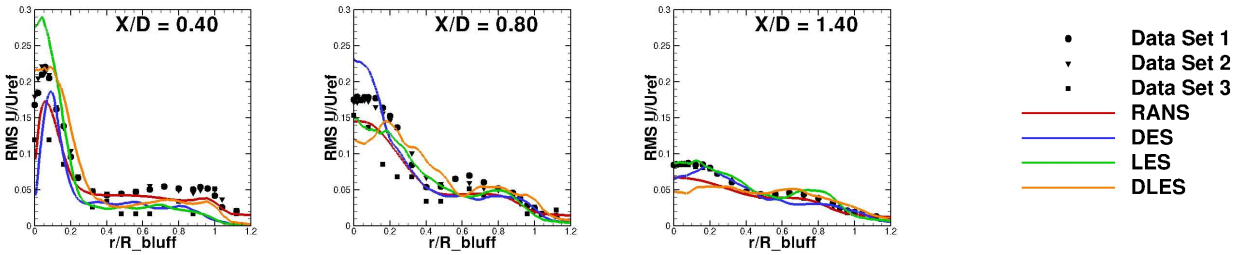

Figure 10. Bluff body burner cold-flow case streamwise RMS velocity comparisons ($\tau_{ii}^{Modelled}$ included).

IV.C. Propane-Jet in Co-Flow

The propane-jet in co-flow case of Schefer[9] features a propane-jet which is exhausted from a relatively skinny pipe into slower co-flowing air with no swirl. This results in shear flow conditions between the jet and co-flow air which influences how the jet diffuses. This case was simulated with RANS, DES, LES, and DLES using structured and unstructured meshes. The structured mesh was comprised of ∼3 600 000 cells and the unstructured mesh was comprised of ∼3 100 000 cells. The structured and unstructured mesh were intended to be as similar as possible in terms as mesh resolution, the layouts of the structured and unstructured meshes are shown in Figures 11 and 12 respectively. Transient simulations were conducted starting from a base RANS flow profile and time marched $T = 0.09s \sim (L/U_{co-flow})$, where L is the simulation domain length in the streamwise direction, once to reach a fully developed flow state and once again to collect steady flow statistics. The time step was chosen to satisfy a CFL condition of unity given $U_{co-flow}$ and the target cell size in the LES focus region.

These simulations were compared with experimental results from Schefer[9] in terms of streamwise velocity, streamwise RMS velocity, and mixture fraction as shown in Figures 14, 15, and 16, respectively, for the structured mesh and Figures 17, 18, and 19 for the unstructured mesh. Results for this case are presented with spacial dimensions scaled using the jet diameter (D), which is 0.0052 m while mean velocities and RMS velocities have been normalized by U_{jet}, which is 53 m/s. Results for this case were primarily compared

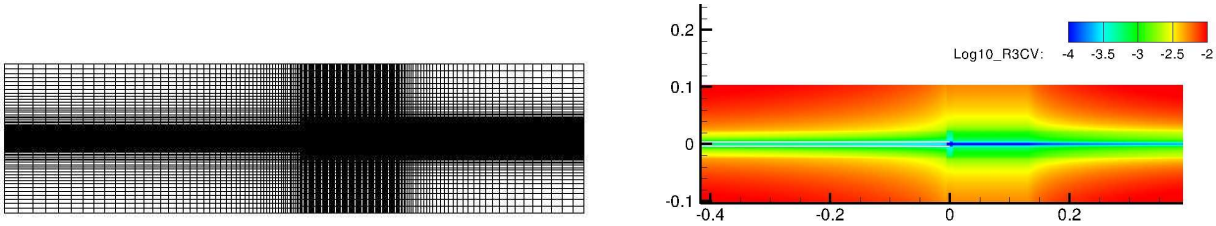

(a) Mesh. (b) Log10 of cubic root of cell volume contours.

Figure 11. Propane-jet in co-flow case structured mesh layout (jet exit at X = 0).

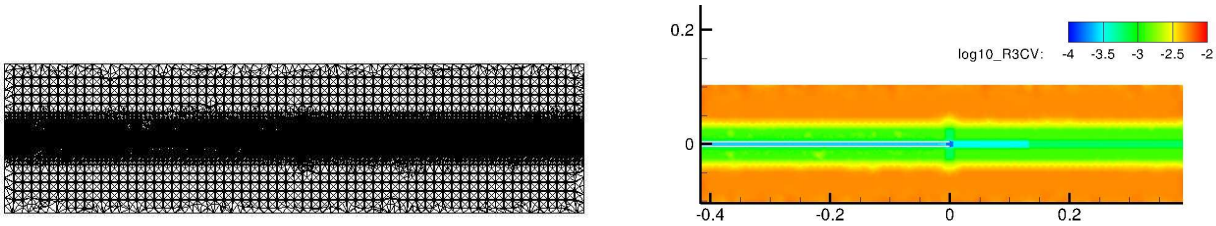

(a) Mesh. (b) Log10 of cubic root of cell volume contours.

Figure 12. Propane-jet in co-flow case unstructured mesh layout (jet exit at X = 0).

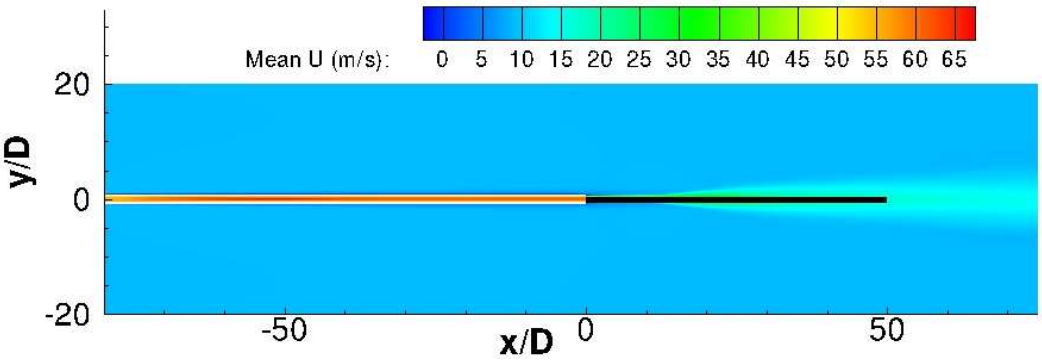

Figure 13. Results comparison station (black) within the mean flow of the propane-jet in co-flow case.

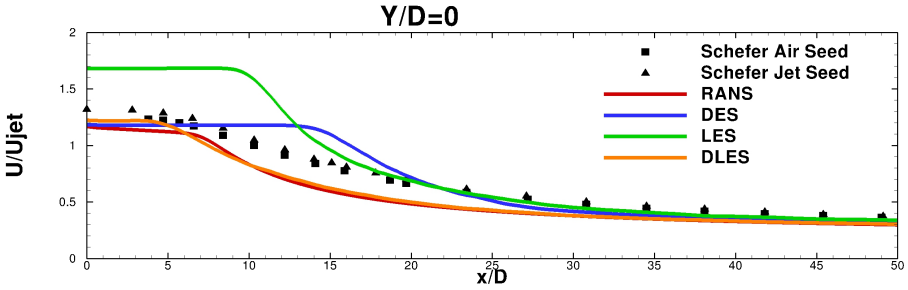

Figure 14. Propane-jet in co-flow streamwise velocity comparison on structured mesh.

along the centerline downstream of the jet as shown in Figure 13.

As can be seen in Figure 20, DES simulations on both the structured and unstructured mesh suffered from MSD. This is despite the fact that, once developed, the resolved TKE was significantly higher than the modelled TKE indicating the mesh was fine enough for LES simulation. Interestingly, the development of resolved TKE seems to have overshot the RANS predictions significantly, possibly compensating to changes in the flow brought about by the delayed transition.

For the structured mesh, as can be seen in Figures 14 and 16, DLES matches RANS the best and is

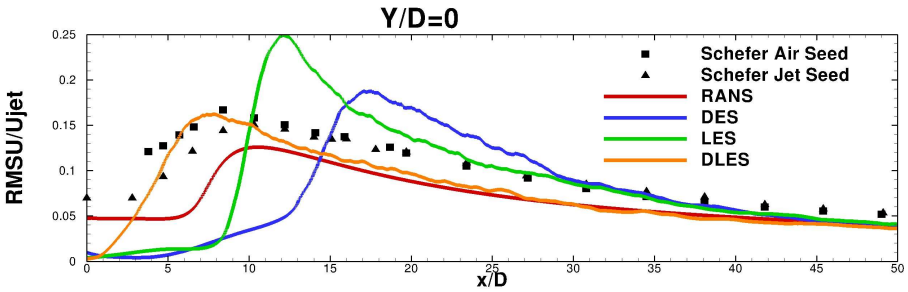

Figure 15. Propane-jet in co-flow streamwise RMS velocity comparison on structured mesh ($\tau_{ii}^{Modelled}$ included).

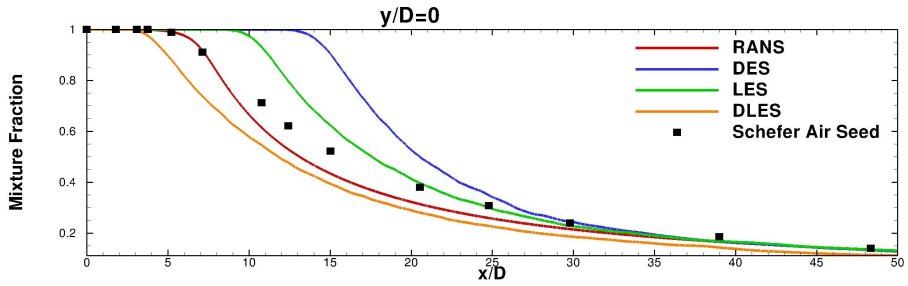

Figure 16. Propane-jet in co-flow mixture fraction comparison on structured mesh.

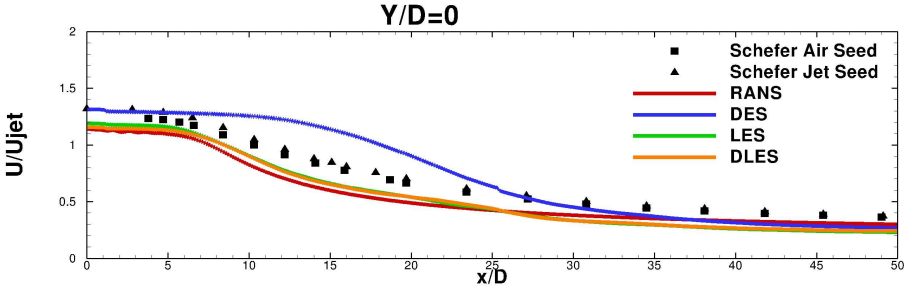

Figure 17. Propane-jet in co-flow streamwise velocity comparison on unstructured mesh.

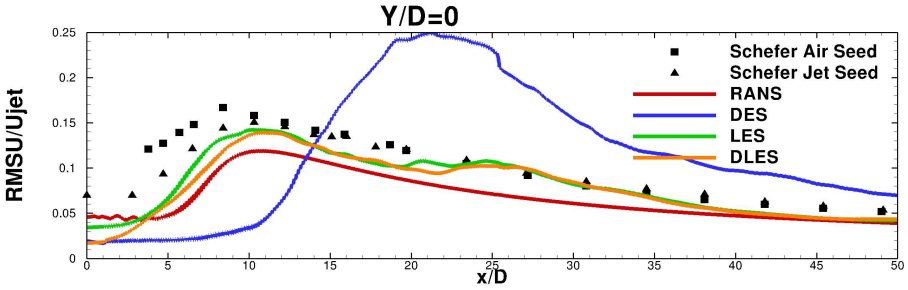

Figure 18. Propane-jet in co-flow streamwise RMS velocity comparison on unstructured mesh ($\tau_{ii}^{Modelled}$ included).

similar to DES in terms of overall agreement with experimental mean velocity and mixture fraction data. However, as seen in Figure 15, DLES matches experimental RMS data the best followed in order by RANS, LES and DES. This is likely because DLES is typically better suited to sheer flows than LES as described in Germano *et al.*[15] while DES is suffering from MSD.

For the unstructured mesh, as can be seen in Figures 17 and 19, DLES and LES match each other closely and are similar to RANS in terms of overall agreement with experimental mean velocity and mixture fraction data with DES being a clear outlier likely due to MSD. As seen in Figure 18, DLES and LES also appear to match each other and experimental RMS data the best followed in order of performance by RANS and DES.

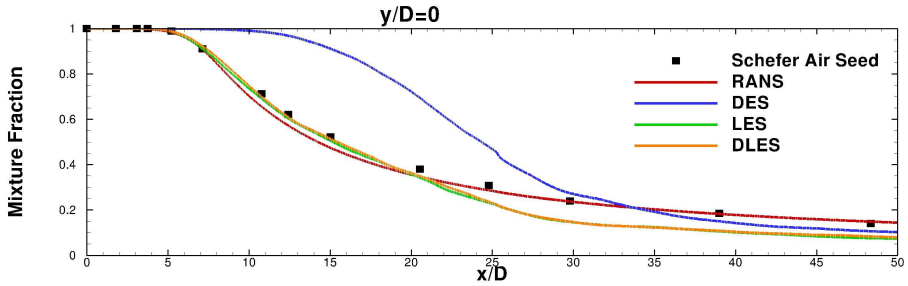

Figure 19. Propane-jet in co-flow mixture fraction comparison on unstructured mesh.

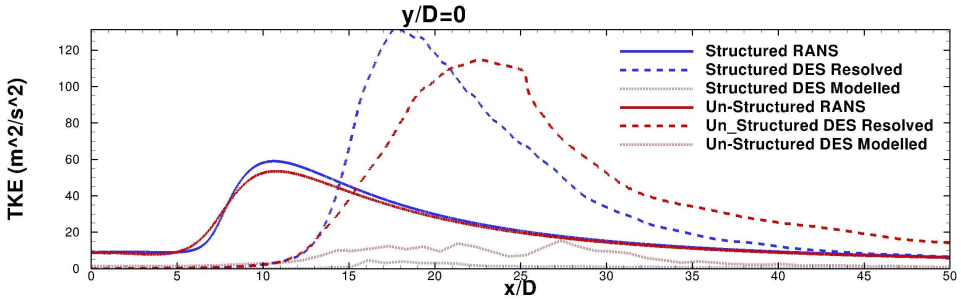

Figure 20. Propane-jet in co-flow TKE comparisons.

IV.D. Hydrogen-Jet in Cross-Flow

For this flow case a small diameter high velocity hydrogen-jet is injected into a rectangular air duct at an angle perpendicular to the slower flowing air. The jet manages to penetrate into the duct flow enough to avoid re-attachment but is ultimately re-directed by the duct flow while mixing. This flow case was simulated with unsteady RANS (URANS), DES, LES, and DLES using a structured mesh of 1 956 664 cells and an unstructured mesh of 2 186 447 cells. The meshing constraints of the geometry results in a pre-LES like mesh configuration for the structured mesh. The unstructured mesh was designed to try and mimic the structured mesh but did not have the same constraints. The mesh layouts of the structured and unstructured meshes are shown in Figures 22 and 23. Simulations were conducted starting from a base steady RANS flow profile and time marched $T = 0.005s \sim (L/U_{cross-flow})$, where L is the simulation domain length in the streamwise direction and $U_{cross-flow}$ is the cross-flow air velocity in the duct, once to reach a fully developed flow state and once again to collect steady flow statistics. The time step was chosen to satisfy a CFL condition of unity given $U_{jet-flow}$ and the target cell size in the LES region, where $U_{jet-flow}$ is the bulk jet flow velocity. A longer section of up-stream duct length consistent with the experimental duct length was simulated using steady RANS, velocity and turbulence property profiles from this steady simulation were used as inlet conditions for the transient simulations.

The hydrogen jet speed was 200 m/s, which is approximately Mach 0.58 in the cross-flow air. As such, simulations were conducted with a compressible solver (density based solver in Ansys FLUENT[19]). URANS was used for comparison as some unsteadiness to this case hindered steady RANS convergence. However, the unsteady behaviour was not very significant. Inspection of instantaneous URANS results appear generally steady and the case could likely be simulated with steady RANS successfully on a coarser mesh. Mean and RMS streamwise velocity profiles for the structured mesh simulations are shown in Figures 24 and 25 respectively and for the unstructured mesh simulations in Figures 26 and 27 respectively. Spatial dimensions were scaled using the jet diameter (D), which is 0.002 m while velocity and RMS velocity values were scaled using $U_{cross-flow}$, which is 55 m/s. Results for this case were primarily compared in profile stations located within the flow as shown in Figure 21.

As can be seen in Figures 24, 25, 26, and 27, although DES performs reasonably well and appears to have an advantage over LES and DLES there does not appear to be an advantage over URANS.

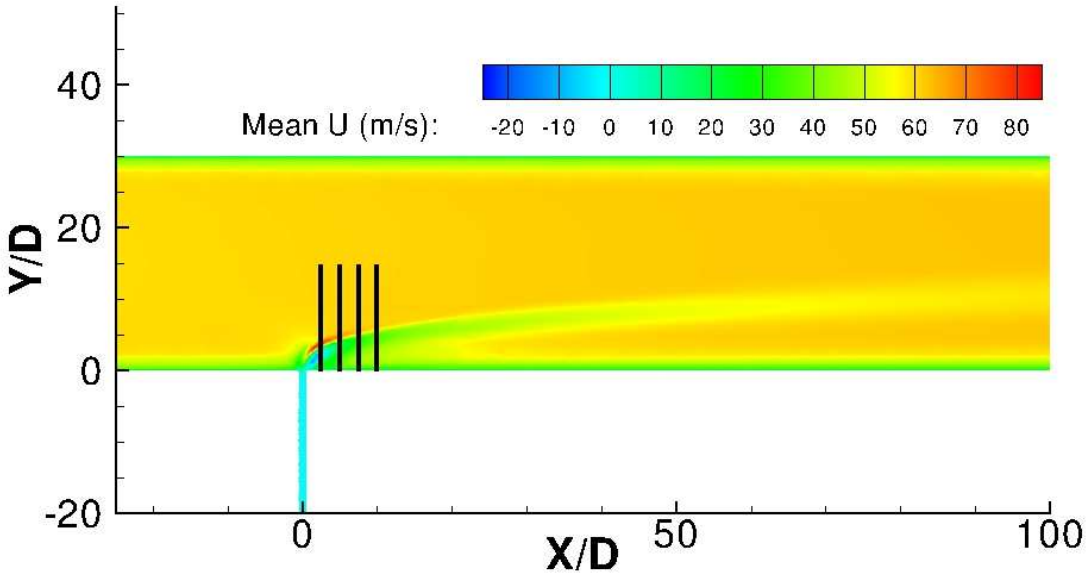

Figure 21. Results comparison stations (black) within the mean flow of the hydrogen-jet in cross-flow case.

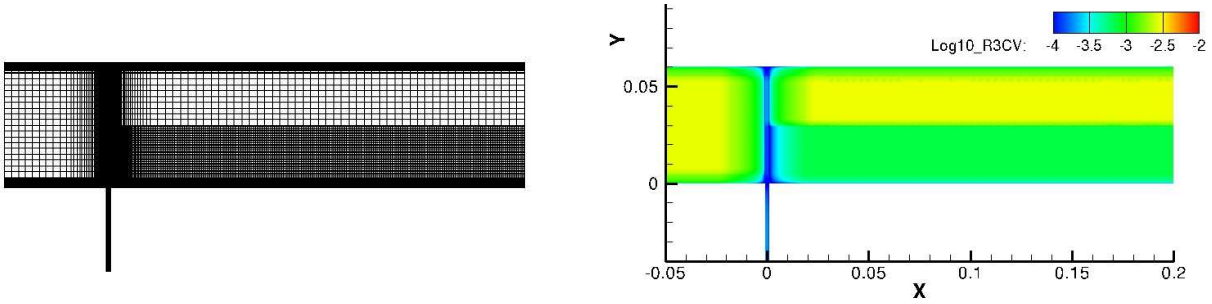

(a) Structured mesh.

(b) Log10 of cubic root of cell volume contours.

Figure 22. Hydrogen-jet in cross-flow structured mesh layout.

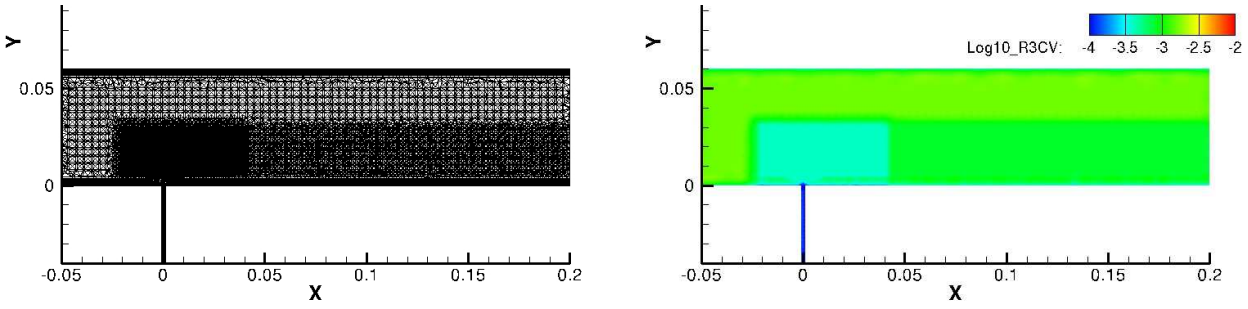

(a) Unstructured mesh.

(b) Log10 of cubic root of cell volume contours.

Figure 23. Hydrogen-jet in cross-flow unstructured mesh layout.

IV.E. Bluff Body Flame Stabilizer in Duct Flow

The bluff body flame stabilizer in duct flow case of Sunjunneson *et al.*[11] utilizes a triangular obstruction in a duct as an analogy of a flame holder. Under cold-flow conditions this case produces vortex shedding phenomenon. Laminar, URANS, DES, LES, and DLES simulations were conducted on a structured mesh

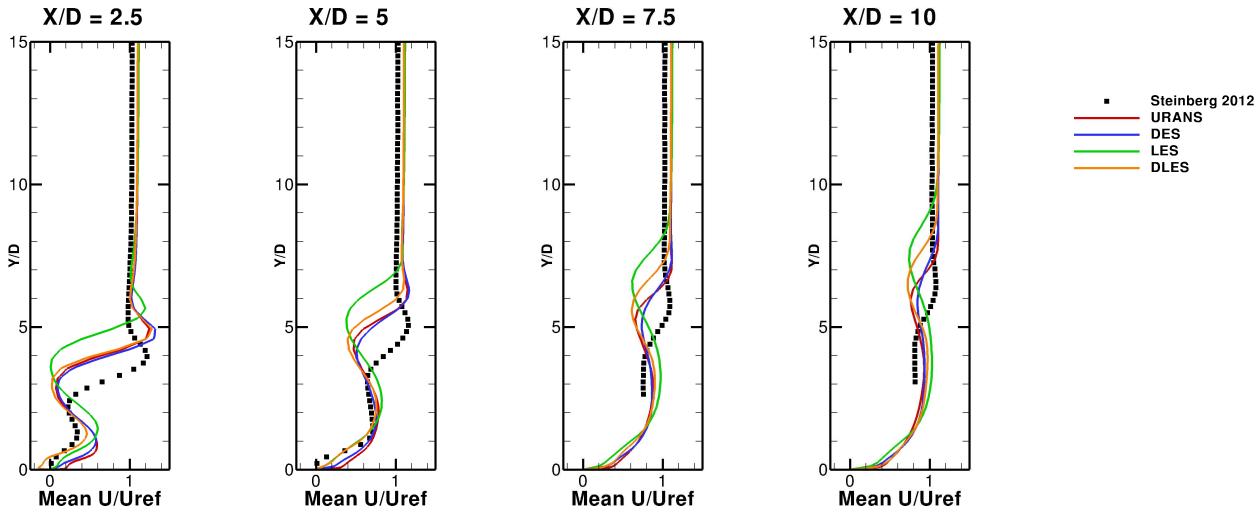

Figure 24. Hydrogen-jet in cross-flow mean streamwise velocity comparisons on structured mesh.

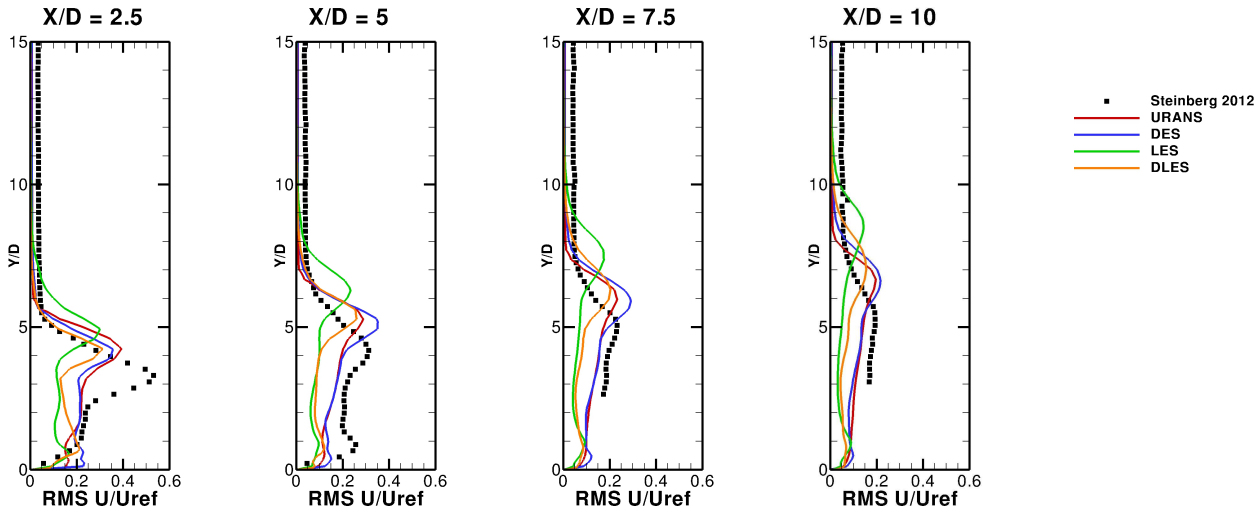

Figure 25. Hydrogen-jet in cross-flow mean streamwise RMS velocity comparisons on structured mesh ($\tau_{ii}^{Modelled}$ included).

containing 872 326 cells, the layout of which is shown in Figure 29. A pressure inlet was utilized instead of a velocity inlet due to the possibility of multiple unsteady modes related to the vortex shedding. Simulations were time marched $T = 0.15s \sim 2\,(L/U_{inlet})$, where L is the simulation domain length in the streamwise direction and U_{inlet} is the case inlet velocity, once to reach a fully developed flow state and once again to collect steady flow statistics. The time step was chosen to satisfy a CFL condition less than unity given U_{max} and the target cell size in the LES region of the mesh, where U_{max} is the highest velocity magnitude identified in the domain. As such, the time step was likely smaller than needed. U_{max} was determined utilizing preliminary steady RANS simulations. The mean and RMS velocity results are shown in Figures 30 and 31 respectively. Spatial dimensions were scaled using the bluff body width (a), which is 0.04 m. Results for this case were primarily compared in profile stations located within the flow as shown in Figure 28.

URANS, DES, LES, and DLES simulations of the bluff body flame stabilizer in duct flow case were also conducted on a unstructured mesh containing 3 628 355 cells. The layout of the unstructured mesh is shown in Figure 32. These simulations utilized a velocity inlet. Additionally, the total simulation time used was $T = 0.375s \sim 5\,(L/U_{inlet})$ prior to collecting flow statistics and again for collecting flow statistics. The mean

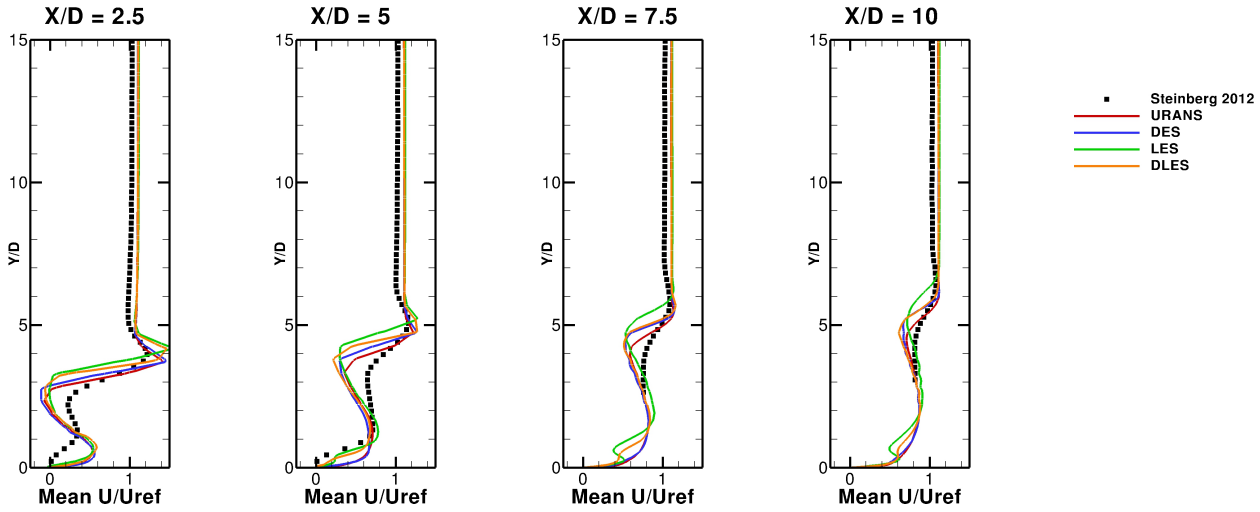

Figure 26. Hydrogen-jet in cross-flow mean streamwise velocity comparisons on unstructured mesh..

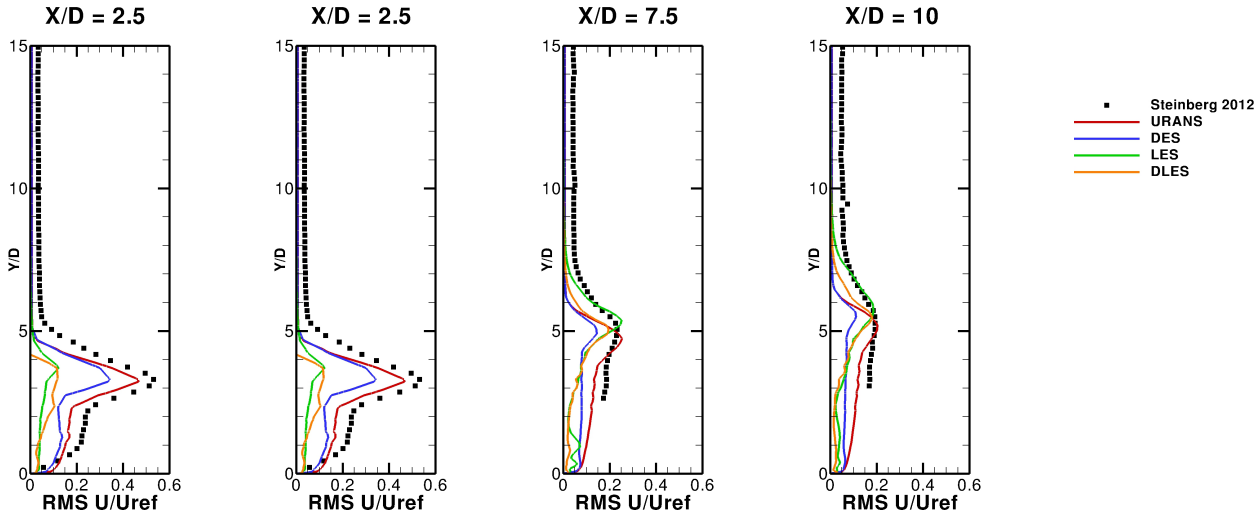

Figure 27. Hydrogen-jet in cross-flow mean streamwise RMS velocity comparisons on unstructured mesh ($\tau_{ii}^{Modelled}$ included).

and RMS velocity results are shown in Figures 33 and 34 respectively.

As can be seen in Figures 30, 31, 33 and 34, for both the structured and unstructured meshes DES, LES, and DLES all produce comparably good results while URANS appears not to work quite as well, particularly for the structured mesh. Interestingly, the laminar simulation on the structured mesh performed well. This suggests that the flow is dominated by the large scale vortex structures and relatively insensitive to sub-grid turbulence.

IV.F. Swirl Stabilized Combustor

As with the other cases, the swirl stabilized combustor was simulated with URANS, LES, DES, and DLES. The domain consists of a complex plenum and swirler assembly prior to a test section where flow measurements were conducted by Steinberg *et al.*[12]. The swirler assembly generates a complex swirling flow entering the text section. A diffuser section was added to the computational domain past the test section to prevent undue interference in the test section from the pressure outlet. Due to the complex geometry,

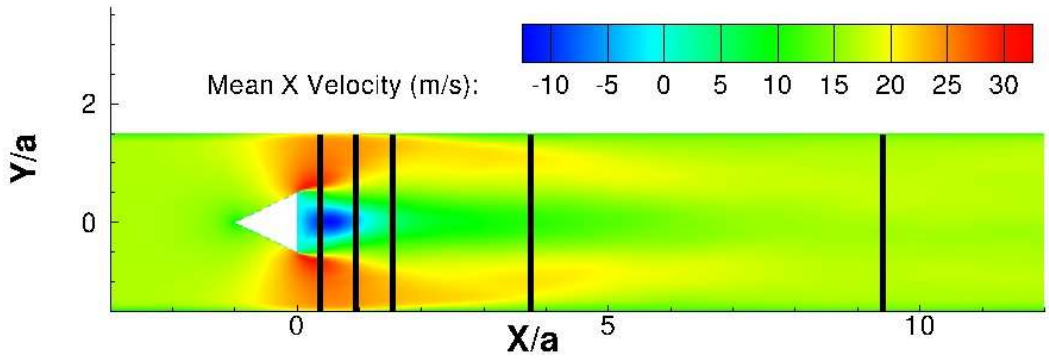

Figure 28. Results comparison stations (black) within the mean flow of the bluff body flame stabilizer in duct flow case.

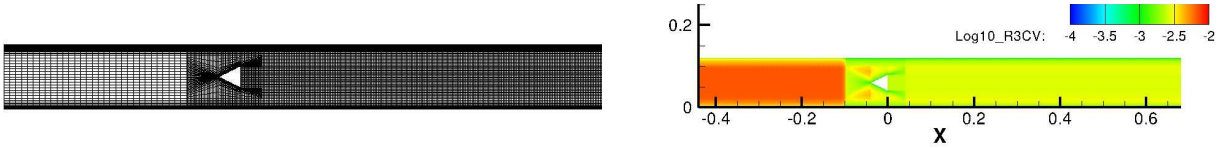

(a) Structured mesh.

(b) Log10 of cubic root of cell volume contours.

Figure 29. Bluff body flame stabilizer in duct flow structured mesh design.

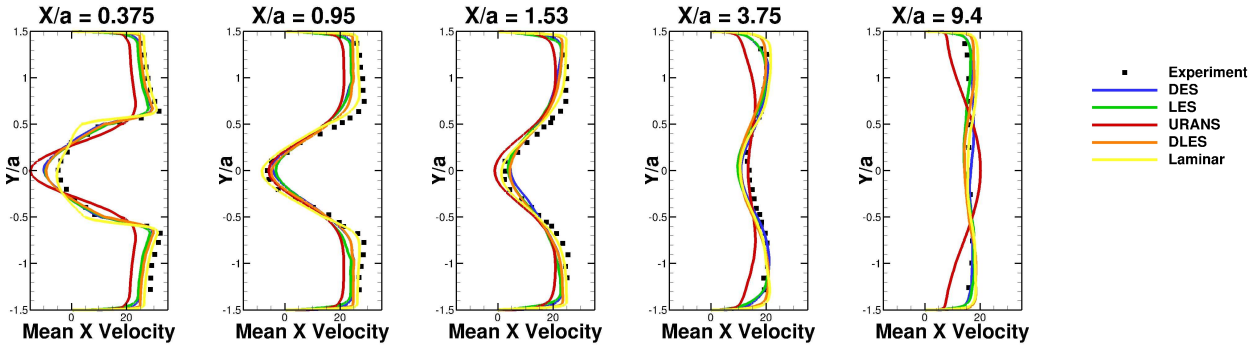

Figure 30. Bluff body flame stabilizer in duct flow structured coarse mesh mean streamwise velocity comparisons (m/s).

an unstructured mesh was used with ∼5 700 000 cells. The unstructured mesh has a tetrahedron dominate interior with prism layers on walls. The mesh design is shown in Figure 36. Simulations were conducted starting from a base steady RANS flow profile and time marched $T = 0.45s \sim 5\,(L/U_{axial})$, where L is the simulation domain length in the streamwise direction and U_{axial} is the volume weighted average axial velocity in the test section, once to reach a fully developed flow state and once again to collect steady flow statistics. The time step was chosen to satisfy a CFL condition of unity given U_{max} and the target cell size in the test section region, where U_{max} is the highest velocity magnitude identified in the domain. Both U_{axial} and U_{max} where determined utilizing preliminary steady RANS simulations. A dense pre-LES region was meshed serendipitously prior to the test section in order to accurately mesh the complex geometry of the swirler assembly. Results for this case were primarily compared in profile stations located within the flow as shown in Figure 35.

These simulations were compared with experimental results from Steinberg *et al.*[12] in terms of streamwise velocity and streamwise RMS velocity, as shown in Figures 37, and 38, respectively. As can be seen in Figures 37 and 38, for this complex geometry case with highly turbulent swirling flows the advantages of

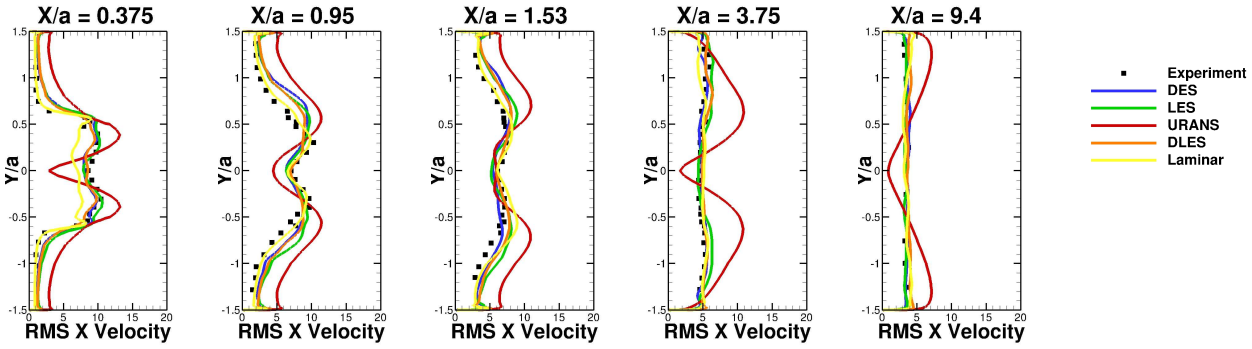

Figure 31. Bluff body flame stabilizer in duct flow structured coarse mesh RMS streamwise velocity ($\tau_{ii}^{Modelled}$ included) (m/s).

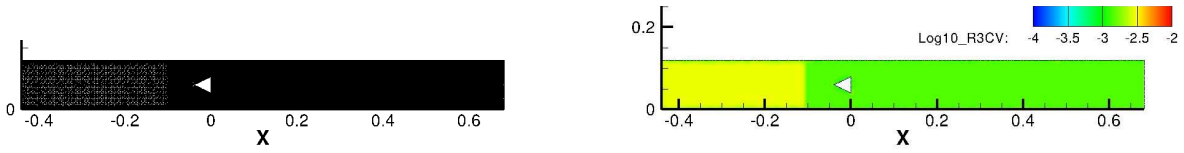

(a) Unstructured mesh.

(b) Log10 of cubic root of cell volume contours.

Figure 32. Bluff body flame stabilizer in duct flow unstructured mesh design.

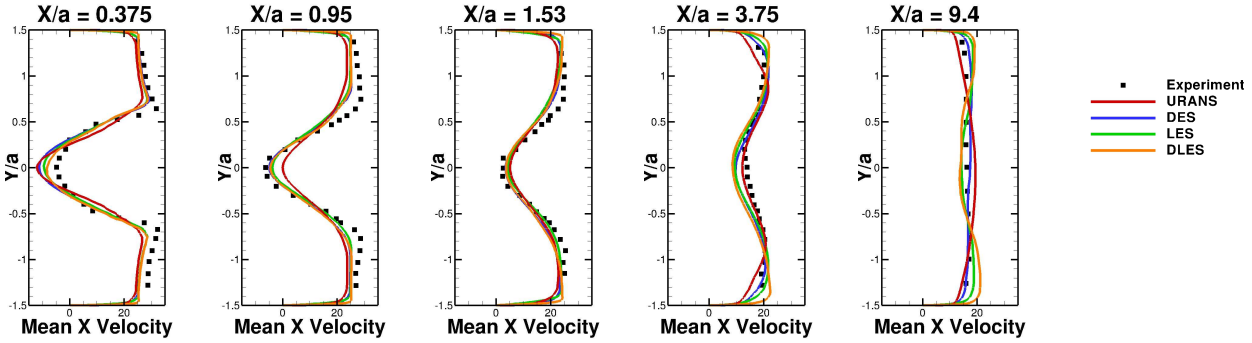

Figure 33. Bluff body flame stabilizer in duct flow unstructured mesh mean streamwise velocity comparisons (m/s).

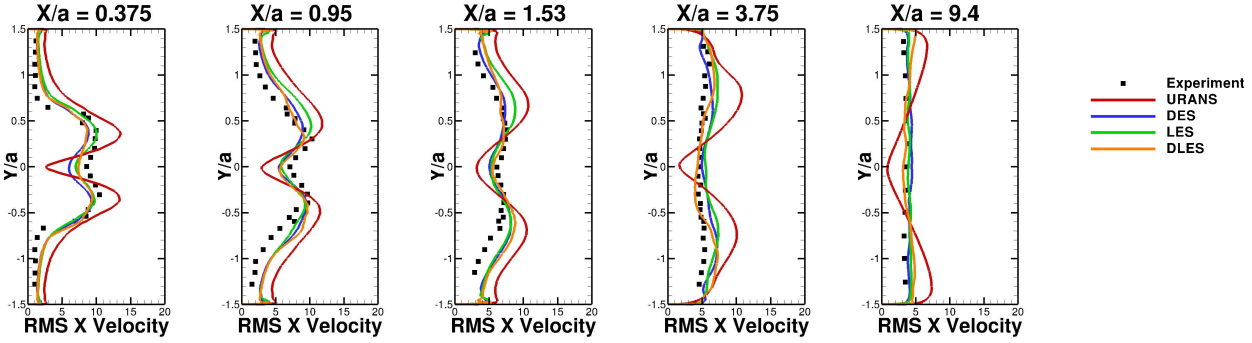

Figure 34. Unstructured mesh mean streamwise RMS velocity comparisons ($\tau_{ii}^{Modelled}$ included) (m/s).

using methods intended to resolve some turbulence over RANS are clear. DES and DLES agree well with each other and the experimental results in terms of the mean velocity profiles. LES does not agree as well as DES or DLES with experimental mean velocity results but still better than RANS. In terms of RMS

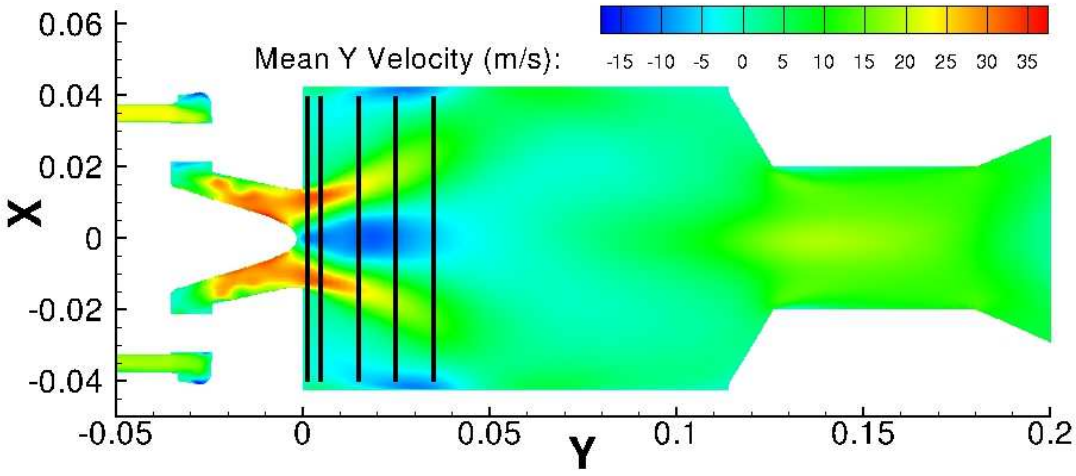

Figure 35. Results comparison stations (black) within the mean flow of the bluff body burner in cold-flow case.

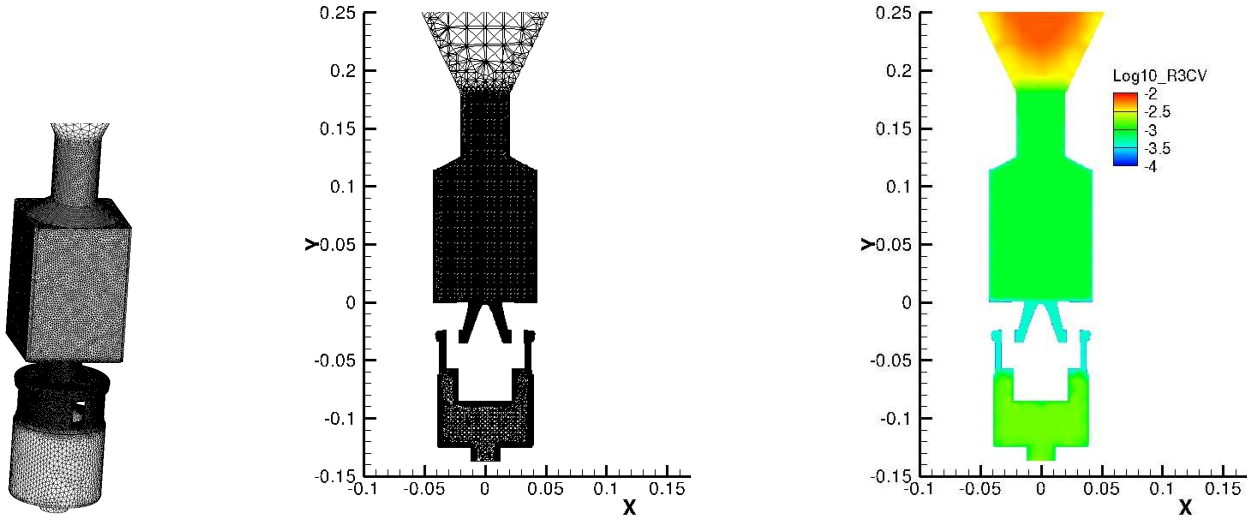

(a) 3D mesh. (b) Plane within mesh. (c) Log10 of cubic root of cell volume.

Figure 36. Swirl stabilized combustor mesh design.

velocity, DES, LES, and DLES all agree very well with each other and reasonably well with experimental results, URANS performance in predicting RMS velocity is a clear outlier.

IV.G. Computational Costs

The total CPU time required to perform each simulation of the six cases over the time frame chosen to collect statistical data for each transient turbulence modelling method is displayed in Table 3. The simulations were conducted using parallel processors, the number of which varied depending on available computational resources. As such the total CPU time is shown instead of wall clock time.

In general, DES was computationally more expensive than LES or DLES. This is likely due to the fact that the DES method used in this study solves two additional equations in the same way a RANS model would. In general, LES was faster than DLES, this is likely because the DLES solution procedure is similar to LES except for the addition of an extra filtering procedure and calculations to evaluate sub-grid scale model performance over a range of resolved scales, as explained in Germano *et al.*[15] However, given the

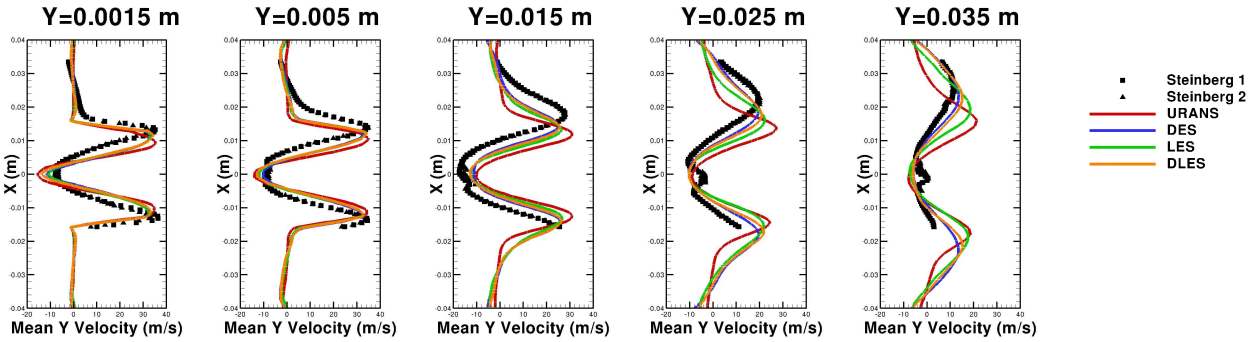

Figure 37. Swirl stabilized combustor mean streamwise velocity comparisons.

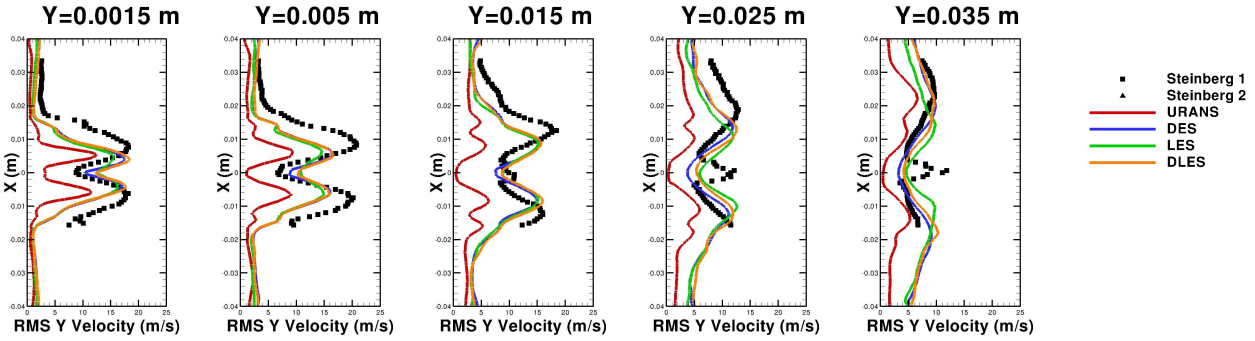

Figure 38. Swirl stabilized combustor streamwise RMS velocity comparisons ($\tau_{ii}^{Modelled}$ included).

Table 3. CPU time required for cold-flow simulations.

Case	Mesh Type	Time (s) *RANS*	Time (s) *URANS*	Time (s) *DES*	Time (s) *LES*	Time (s) *DLES*
B.F.S.	*Structured*	24 623	-	2 439 663	1 451 760	1 771 400
Propane Jet	*Structured*	2 262 078	-	27 217 704	23 588 862	25 855 523
Propane Jet	*Unstructured*	929 591	-	6 628 841	7 331 543	8 141 921
Hydrogen Jet	*Structured*	-	3 417 615	7 455 490	5 613 624	1 435 547
Hydrogen Jet	*Unstructured*	-	1 456 747	1 468 546	1 351 885	1 427 183
S.S.C.	*Unstructured*	-	4 166 181	25 825 074	3 693 307	3 980 829
B. B. Flame Stabilizer	*Structured*	-	130 999	324 649	188 354	356 492
B. B. Flame Stabilizer	*Unstructured*	-	1 402 607	3 409 071	3 042 419	1 068 420
B. B. Burner	*Structured*	586 441	-	566 908	782 655	697 997

number of cases and the use of sub-iterative convergence criteria as the basis for time step advancement, there was significant variation from these trends which for the most part didn't appear to impact results. For example, for the swirl stabilized combustor case, LES is the fastest method followed closely by DLES. DES for the swirl stabilized combustor was anomalously slow, for that simulation the sub-iterative convergence procedure was limited by the k equation which is not considered for LES or DLES. It is likely that this extra cost was unnecessary and a more comparable simulation time could be obtained by re-simulating the case without assigning a convergence limit to the k equation.

Since similar time stepping and meshing requirements are required for all LES like transient methods, these turbulence modelling simulation types should be considered generally comparable in terms of simulation time unless the modeller has enough experience with the case at hand to know what sub-iterative convergence behaviour is likely from each model.

V. Conclusions

Although DES is a promising method for integrating the boundary layer modelling capability of RANS with the large-scale turbulent structure modelling ability of LES, its performance in comparison to stand-alone methods can be degraded due to established DES deficiencies such as MSD for simple flows that analogize features of practical gas-turbine combustors. However, user knowledge of the MSD problem and manipulation of the mesh, through a pre-LES zone, to alter the size and location of the MSD region can significantly improve performance and the accuracy of the predicted results, at least for the combustor-relevant cold-flows of interest here. Additionally, the disadvantages of DES, such as MSD, do not appear to be as detrimental to complex highly turbulent and swirling flows, which are more representative of the flows of interest occurring in practical gas-turbine combustor configurations.

Additionally, RANS methods proved robust for many of the simpler flows considered. Although DES, LES, and DLES could be made to match RANS performance for these simpler cases, it was not until more complicated flow features such as high swirl and/or flow unsteadiness were introduced that hybrid RANS/LES methods and other transient turbulence-resolving methods demonstrated clear advantages over RANS for the cases considered. This finding is somewhat contrary to the expectations of gradual degradation in the performance of RANS methods with increasing flow complexity. Nevertheless, for swirling three-dimensional and highly unsteady flows (representative of practical gas turbine combustor flows), DES is clearly shown to be superior to RANS and/or URANS approaches.

Acknowledgements

Computations were primarily performed on the GPC supercomputer at the SciNet HPC Consortium. SciNet is funded by: the Canada Foundation for Innovation under the auspices of Compute Canada; the Government of Ontario; Ontario Research Fund - Research Excellence; and the University of Toronto.

Financial support for this project was primarily provided by Pratt & Whitney Canada and NSERC through their Industrial Research Chair in Aviation Gas Turbine Combustion/Emissions Research and Design System Optimization program. Additional financial support was provided by the International Society of Transport Aircraft Trading through their scholarship program.

References

[1]Wilcox, D., *Turbulence Modeling for CFD Third Eddition*, DWZ Industries, Inc., La Canada, California, 3rd ed., 2006.

[2]Fröhlich, J. and von Terzi, D., "Hybrid LES/RANS Methods for the Simulation of Turbulent Flows," *Progress in Aerospace Sciences*, Vol. 44, No. 5, 2008, pp. 349–377.

[3]Spalart, P., "Detached-Eddy Simulation," *Annual Review of Fluid Mechanics*, Vol. 41, 2009, pp. 181–202.

[4]Choi, J., Yang, V., Ma, F., and Jeung, I., "Detached Eddy Simulation of Combustion Dynamics in Scramjet Combustors," *Joint Propulsion Conference and Exhibit*, 43, AIAA/ASME/SAE/ASEE, 2007.

[5]Sainte-Rose, B., Bertier, N., Deck, S., and Dupoirieux, F., "Delayed Detached Eddy Simulation of a Premixed Methane Air Flame Behind a Backward Facing Step," *Joint Propulsion Conference and Exhibit*, 44, AIAA/ASME/SAE/ASEE, 2008.

[6]Sainte-Rose, B., Bertier, N., Deck, S., and Dupoirieux, F., "A DES Method Applied to a Backward Facing Step Reactive Flow," *Comptes Rendus Mcanique*, Vol. 337, No. 6-7, 2009, pp. 340–351.

[7]Driver, D. and Seegmiller, L., "Features of a Reattaching Turbulent Shear Layer in Divergent Channel Flow," *AIAA Journal*, Vol. 23, No. 2, 1985, pp. 163–171.

[8]Dally, B., Fletcher, D., and Masri, A., "Flow and Mixing Fields of Turbulent Bluff-Body Jets and Flames," *Combustion Theory and Modelling*, Vol. 2, No. 2, 1998, pp. 193–219.

[9]Schefer, R., "Data Base for a Turbulent, Nonpremixed, Nonreacting Propane-Jet Flow," Tech. rep., Sandia National Laboratories Combustion Research Facility, Livermore, California, 12 2011.

[10]Steinberg, A., Sadanandan, R., Dem, C., Kutne, P., and Meier, W., "Structure and Stabilization of Hydrogen Jet Flames in Cross-Flows," *Proceedings of the Combustion Institute*, Vol. 34, No. 1, 2013, pp. 1499–1507.

[11]Sjunnesson, A., Nelsson, C., and Max, E., "LDA Measurements of Velocities and Turbulence in a Bluff Body Stabilized Flame," *Laser Anemometry*, Vol. 3, 1991, pp. 83–90.

[12]Steinberg, A., Arndt, C., and Meier, W., "Parametric Study of Vortex Structures and their Dynamics in Swirl-Stabilized Combustion," *Proceedings of the Combustion Institute*, Vol. 34, No. 2, 2013, pp. 3117–3125.

[13]Menter, F., Kuntz, M., and Langtry, R., "Ten Years Industrial Experience with the SST Turbulence Model," *In Turbulence, Heat and Mass Transfer*, edited by K. Hanjalić, Y. Nagano, and M. Tummers, Begell House, Inc., 4th ed., 2003, pp. 625–632.

[14]Piomelli, U., "Large-Eddy Simulation: Achievements and Challenges," *Progress in Aerospace Sciences*, Vol. 35, 1999, pp. 335–362.

[15]Germano, P., Piomelli, U., Moin, P., and Cabot, W., "A Dynamic Subgrid-Scale Eddy Viscosity Model," *Physics of Fluids*, Vol. 3, No. 7, 1991, pp. 1760–1765.

[16]Patankar, S. and Spalding, S., "A Calculation Procedure for Heat, Mass and Momentum Transfer in Three-Dimensional Parabolic Flows," *International Journal of Heat and Mass Transfer*, Vol. 15, 1972, pp. 1787–1806.

[17]Barth, T. and Jespersen, D., "The Design and Application of Upwind Schemes on Unstructured Meshes," *Aerospace Sciences Meeting*, No. AIAA-89-0366 in 27, AIAA, 1989.

[18]Spalart, P., "Young-Person's Guide to Detached-Eddy Simulation Grids," Contractor Report NASA/CR-2001-211032, NASA, 2001.

[19]ANSYS, Inc., Canonsburg, Pennsylvania, *ANSYS FLUENT User's Guide*, 13th ed., 2010.